Showcasing research from Professor Jae Sung Yoon's laboratory, Nano Lithography and Manufacturing Research Center, Korea Institute of Machinery and Materials (KIMM), Daejeon 34103, Korea.

Anti-counterfeiting labels of photonic crystals with versatile structural colors

Close-packed and non-close-packed monolayers of nanoparticles are integrated onto commercial tape to facilitate an overt–covert photonic crystal. The hidden label is revealed only under specific external triggers, such as attaching or removing a transparent cover film. This label is demonstrated in various anti-counterfeiting applications, including water-responsive labels and multi-layer authentication, which enhance the security level and versatility of this study.

ROYAL SOCIETY OF **CHEMISTRY**

rsc.li/nanoscale-advances

PAPER

Check for updates

Anti-counterfeiting labels of photonic crystals with versatile structural colors†

Nguyen Hoang Minh, [ID] ab Kwanoh Kim,a Do Hyun Kang,a Yeong-Eun Yooab and Jae Sung Yoon*ab

Labels with structural color based on photonic crystals (PCs) have drawn significant attention due to their unique color emission, offering promising solutions for anti-counterfeiting applications. However, to meet the demands of future high-security applications, conventional structural color labels require further improvement. This study introduces a novel approach to fabricate highly encrypted anti-counterfeiting labels by combining close-packed and non-close-packed monolayers of nanoparticles (NPs) onto adhesive surfaces. The photonic crystals, arranged in specific geometric shapes, exhibit overt–covert characteristics. The hidden label is only revealed under specific external triggers, such as attaching or removing a transparent cover film. The principle of color modulation of the photonic crystal is elucidated, highlighting the role of packing density and refractive index matching. Additionally, the scalability and cost-effectiveness of the fabrication process in this study are expected to facilitate future commercialization. Various anti-counterfeiting applications, including water-responsive labels and multi-layer authentication, are demonstrated also, which enables higher security levels and versatility of this study.

Introduction

Counterfeiting has become a significant problem to global economies, public health, and social development,[1,2] causing financial losses of 2 trillion USD in 2021.[3] To solve this problem, various anti-counterfeiting methods have been studied including barcodes,[4,5] watermarks,[6] luminescence,[3,7,8] and laser encoding.[9,10] Among these, structural color labels based on photonic crystals (PCs) have gained considerable attention due to their optical properties and potential for enhanced security.[11–15] The structural color is generated by the optical interaction of light with micro- or nano-structures, such as diffraction, interference, and scattering.[16] According to Bragg's law, the reflected wavelength is determined by the incident and viewing angles, the lattice constant, and the refractive index.[17] Artificial photonic crystals inspired by natural examples exhibit unique angle-dependent colors and have been widely employed for anti-counterfeiting applications.[18,19] However, most iridescent labels remain constantly visible, limiting their effectiveness in high-security applications. Therefore, recent research has focused on encrypted, multi-mode photonic crystals[3,16,20–22] that become visible only when triggered by external stimuli, known as responsive PCs.[22–25]

Responsive PCs remain invisible under normal conditions but become visible when exposed to stimuli like water or solvent,[26–28] heat,[29,30] mechanical deformation,[31–33] and photo-luminescence.[34,35] The colors of the photonic crystal change due to variations in the lattice constant or the mean refractive index, making the hidden label visible.[36,37] For example, Wu *et al.* reported a programmable thermochromic PC label *via* customizing the heat-responsive properties of the PC film.[38] When the temperature dropped, the effective refractive index of the film changed locally, leading to the revelation of a covert label. In another approach, a PC encrypted in h-SiO$_2$/PU PC was created by Zhang *et al.* for the anti-counterfeiting labels.[20] The diffusion of the specific solvent into the local PC caused the difference in refractive indices between the label and the surrounding area, resulting in the appearance of the label. However, previous techniques are based on the opal or inverse opal structures, which are challenging to fabricate uniformly on a large scale. An ideal encrypted PC label for commercialization needs to fulfill the following criteria.

(i) Covert feature: the difference between the labels and the surrounding area must be minimized to ensure that the label remains hidden.

(ii) High contrast under activation: when activated by external stimuli, the color contrast should be sufficiently high to clearly reveal the hidden label.

(iii) Practical stimuli and decoding: the required stimuli should be readily available in ordinary conditions and settings, and the decoding process should be straightforward and rapid.

aNano Lithography and Manufacturing Research Center, Korea Institute of Machinery and Materials (KIMM), Daejeon 34103, South Korea. E-mail: jaesyoon@kimm.re.kr

bDept. Nanomechatronics, University of Science and Technology (UST), Daejeon 34113, South Korea

(iv) Cost-effective and scalable fabrication: the fabrication process must be economical and scalable for commercial production.

In this study, a facile technique meeting the above requirements is introduced to fabricate multiple-state anti-counterfeiting labels. By integrating nanoparticle monolayers with different packing densities onto a flexible adhesive tape, we demonstrate a unique overt–covert feature. When the nanoparticles are closely packed, the label remains visible. But when they are arranged with low packing density, the label becomes hidden with mechanical pressure. This approach maintains a consistent color and viewing angle while offering a novel and commercially viable method for highly encrypted anti-counterfeiting labels.

Method

Preparation of close-packed and non-close-packed monolayers of NPs

Fig. 1 shows the fabrication processes for close-packed and non-close-packed monolayers of NPs. Two kinds of NPs were used for the experiments in this study, which are polystyrene (PS) with a diameter of 780 nm (Bangs Laboratories, Inc.) and polymethyl methacrylate (PMMA) with a diameter of 700 nm (CD Bioparticles) (Fig. S1†). Monolayers of NPs were assembled on a silicon wafer by 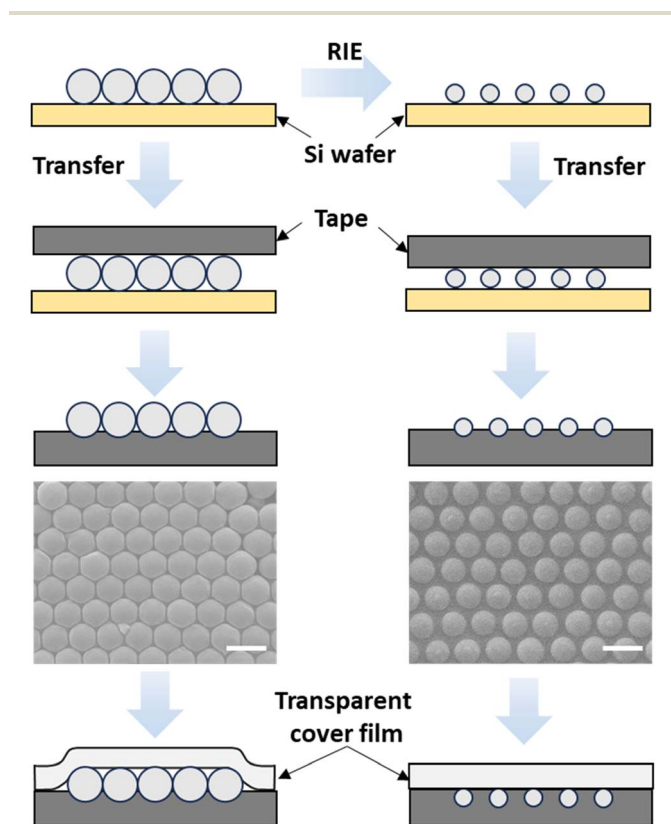spin coating and dip coating methods as reported in numerous studies.[13,39] First, a silicon substrate was treated with oxygen plasma to obtain a super-hydrophilic surface. Subsequently, in the spin coating process, 100 µl of PS or PMMA nanoparticles (10% wt/v) were dropped on the Si substrate, followed by spinning at various speeds (600–1600 rpm). Then, monolayers of nanoparticles were obtained with various area fractions of surface coverage. Meanwhile, the dip coating method was also employed to fabricate the monolayer of nanoparticles with 100% area fraction. In this method, the PS nanoparticle solution (10% wt/v) was mixed with IPA at a ratio of 1 : 1. Subsequently, the monolayer of nanoparticles was dispersed on the water–air interface by injecting the mixture slowly with a syringe at a speed of 100 µl min^{-1}. After that, a few drops of SDS surfactant were added to enhance the crystallization and remove the voids in the monolayer. This monolayer was transferred onto the Si substrate by withdrawing the substrate from the water–air interface. Initially, the NPs were self-assembled into a close-packed monolayer (CPM). Then, the non-close-packed monolayer (NCPM) of NPs was obtained by etching them with the reactive ion etch (RIE) technique at a power of 80 W for etching time from 60 to 85 s. Subsequently, two types of monolayers of NPs were fabricated on silicon substrates. These layers were transferred onto black or transparent adhesive tapes (83100H/6450BZ, Horae) through a shadow mask (stainless steel, 100 µm thick), resulting in the formation of PCs in the designed geometric areas. And a polyethylene terephthalate (PET) film (100 µm thick) was used as a transparent cover film.

Characterization

The morphology of PCs was observed and measured using a scanning electron microscope (SEM, SM-356, Topcon Corp.). The wavelength of the reflected light from the PCs was measured using a spectrometer (Flame-s-*vis*-nir, Ocean optics, Inc.) on a customized stage. The photos and videos were taken using the camera of iPhone. And the images of the monolayer

Fig. 1 Schematic of the fabrication processes and SEM images of close-packed and non-close-packed monolayers of nanoparticles on the flexible adhesive tape (scale bar: 1 µm).
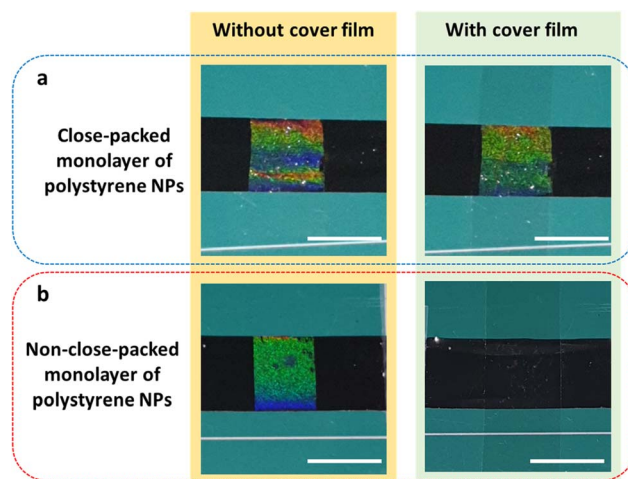

Fig. 2 Labels with (a) close-packed, and (b) non-close-packed monolayer of polystyrene NPs on black tape before and after application of a transparent cover film (scale bar: 1 cm).

were captured by an Optical Microscope (BX53MRF-S, Olympus) and analyzed using software (ImageJ, U. S. National Institutes of Health).

Results and discussion

Close-packed and non-close-packed monolayers of polystyrene NPs were obtained, with diameters of 780 nm and 710 nm, respectively. Then they were transferred onto the flexible tapes as seen in Fig. 2, Videos S1 and S2.† These results show that both of the PCs emitted iridescent structural colors. However,
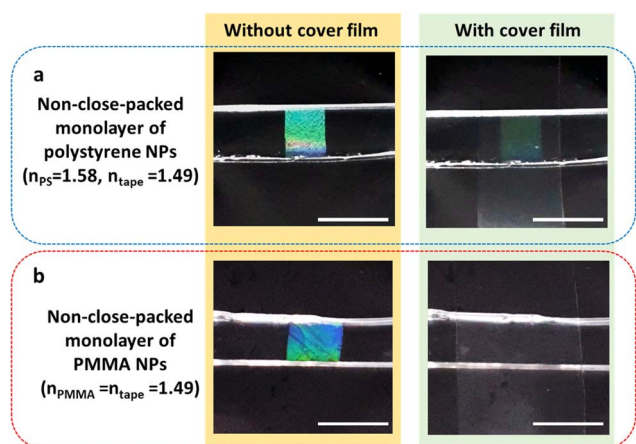

Fig. 3 Labels with non-close-packed monolayers of (a) polystyrene NPs, and (b) polymethyl methacrylate NPs on transparent tape before and after application of a transparent cover film (scale bar: 1 cm).

the color from the NCPM disappeared while that from the CPM remained stable when a transparent cover film was applied on the surface. This difference was caused by the size and packing density of the particles, as illustrated in Fig. 1. If the particles are small and sparsely arranged, they are buried beneath the surface of the adhesive tape by application of the cover film. And there are sufficient voids between the particles, ensuring adhesion between the film and tape, so that the particles cannot be extruded but remain embedded under the surface of the tape. Meanwhile, the particles in the close-packed layer cannot be buried fully by application of the cover film. And the film and tape are not in contact within the perimeter of the monolayer due to the lack of voids between particles. Therefore, the CPM showed the structural color even after the cover film was applied. As previously discussed, packing density has been identified as a significant parameter influencing the response of PCs when subjected to mechanical pressure in the presence of a transparent cover film. Additionally, the light absorbance of the adhesive tape and the refractive indices of both the PCs and the tape are also important factors when the particles are embedded beneath the surface of the tape. In order to investigate these parameters, experiments were conducted with non-close-packed layers of PS and PMMA nanoparticles on the transparent adhesive tapes as seen in Fig. 3 and Video S3.† The particles in these results are not close-packed, so they can be assumed to be buried or embedded beneath the surface of tape with application of the cover film. But Fig. 3a shows that color from PS particles still remained with decreased intensity. Since the adhesive tape is transparent, incident light reaches the particles beneath the surface of the tape resulting in optical interactions for structural color, which was inhibited on the
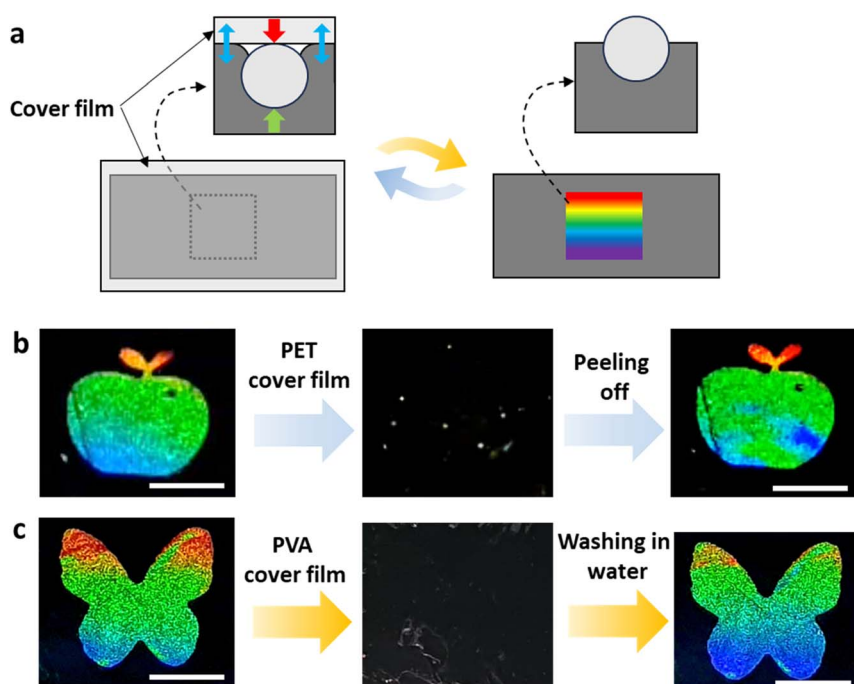

Fig. 4 (a) Illustration of embedment or extrusion of nanoparticles on adhesive tape, (b) revelation of the label by peeling off the cover film, and (c) revelation of the label by dissolving the cover film (scale bar: 1 cm).

black tape. And the refractive indices of PS and the tape are 1.58 and 1.49, respectively. This difference also caused the remaining color of PCs after they are embedded beneath the surface. So, when the refractive indices were matched by using PMMA particles (refractive index = 1.49), the PCs became completely covert after the cover film was applied, as seen in Fig. 3b and Video S4.† These results suggest that the overt–covert feature of PCs could be obtained by the principle of this study. And it is shown that the refractive indices of the particles and tape don't need to be matched on the black tape, while they need to be matched on the transparent one.

Notably, this overt–covert process is reversible, as the colors reappear after the cover film is peeled off. Fig. 4a shows the schematics of overt and covert states. With the cover film, the particles are embedded under the surface with deformation of the tape. At this state, the forces acting on particles are in equilibrium, which are the elastic restoration of the tape (green arrow) and the reaction force by the cover film (red arrow) caused by adhesion force between the tape and film (blue arrows). When the cover film is removed, the reaction force vanishes. Thus, the particles are partially extruded out of the surface by the elastic restoration of the tape, resulting in iridescent colors. Fig. 4b and Video S5† show a demonstration of this principle as an anti-counterfeiting label for several tests, whose transition of visibility is reliably effective and reversible.

As described above, the hidden or covert label is revealed by the removal of the PET cover film. So further experiments were done by replacing the transparent cover film with a thin polyvinyl alcohol (PVA) film. Since PVA is soluble in water, this cover film can be removed by dipping in or washing with water. As seen in Fig. 4c and Video S6,† a geometric shape (butterfly) was hidden with the PVA cover film, but it was restored with its colors after being washed in water. Therefore, the working principle in this study also presents a feasible approach for developing water-responsive anti-counterfeiting labels.

The photonic crystals in this study emit vivid and iridescent colors resulting from the diffraction of incident light, which is based on Bragg's law. The color is caused by the difference of optical paths of 2 adjacent light beams, which is expressed in the equation[19] (Fig. S2†).

$$\Delta = nd (\sin \theta_1 + \sin \theta_2) \tag{1}$$

where θ_1, and θ_2 are the incident and diffraction angles, respectively, and n is the refractive index of the surrounding environment (1 for the ambient air). d is the lattice constant or distance between adjacent lattice rows, which is equal to $\sqrt{3}/2D$ (D is the distance between centers of two adjacent nanostructures). For the close-packed hexagonal NPs, D is the diameter of NPs. When the difference of optical paths (Δ) is equal to the integer multiple (m) of a certain wavelength (λ), constructive interference occurs at this wavelength as described by the following equation.
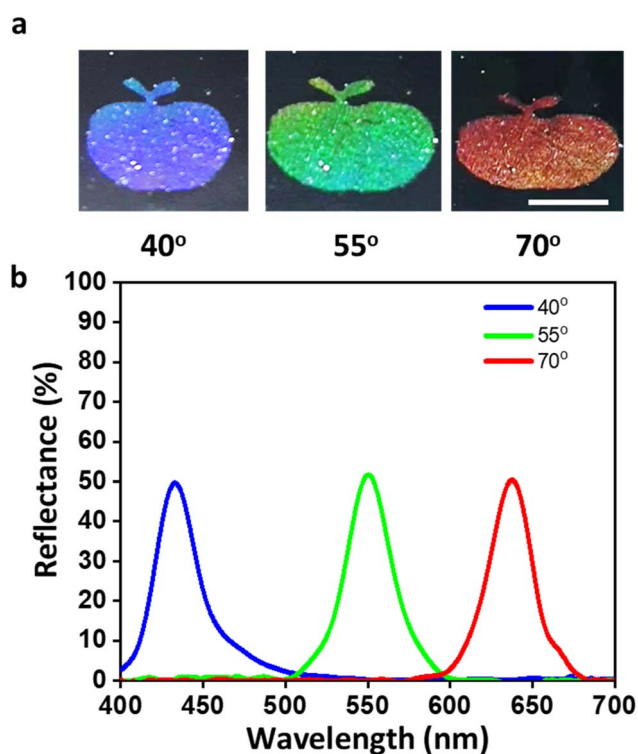

Fig. 5 Angle dependency of photonic crystals of PS nanoparticles on a black adhesive tape. Pictures (a) and reflectance profiles (b) for various viewing angles (scale bar: 1 cm).
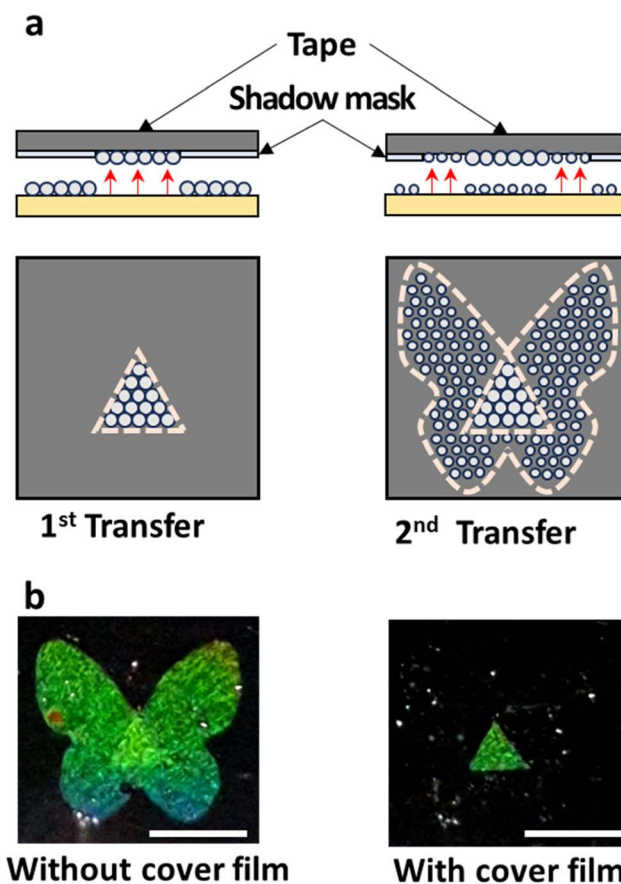

Fig. 6 (a) Fabrication process of hybrid labels with integration of the CPM and NCPM, and (b) encrypted and revealed shape (triangle) (scale bar: 1 cm).

$$m\lambda = nd\,(\sin\theta_1 + \sin\theta_2) = \sqrt{3}/2D\,(\sin\theta_1 + \sin\theta_2) \qquad (2)$$

As a result, PC emits colors when the diffracted wavelength is within the visible spectrum. In this study, the diameter of NP (D) is 780 nm, and the light source is fixed at the normal direction to the surface of the substrate ($\theta_1 = 0°$). So diffracted wavelength is calculated to be 434, 553, and 635 nm at θ_2 of 40°, 55°, and 70°, respectively. These values align well with the experimental results as shown in Fig. 5.

As shown in eqn (2), the colors are determined by the angles and the lattice constant. And the photonic crystals of the CPM and NCPM in this study have the same lattice constant (780 nm), so they show the same colors if they are observed at the same angle. This offers us another strategy to fabricate an overt–covert label for anti-counterfeiting usage, which is the encrypted label.[30,31] The encrypted label in this study was obtained by integrating the CPM and NCPM into a hybrid label, as illustrated in Fig. 6a. First, the CPM was transferred onto an adhesive tape using a shadow mask with a triangle-shaped opening. Next, the NCPM was transferred onto the same tape using a shadow mask with a butterfly-shaped opening. In this step, the NCPM was transferred within the butterfly except the triangle, because the triangle was already occupied by the CPM. As a result of the same lattice constant, the colors of both the

CPM and NCPM are identical at arbitrary angles. Therefore, the triangle is hardly recognizable without the cover film in Fig. 6b. This is not because its color disappeared but because it had the same color with the surrounding area. But the triangle became clear after application of the cover film as the color of the butterfly faded out. However, this result also shows that the triangle was not completely hidden even without the cover film (Fig. 6b). Although the CPM and NCPM originate from the same monolayer of NPs and have identical lattice constants, their diameters differ. This leads to the difference in intensity of diffracted color, making the triangle shape slightly visible. So further investigation was conducted on the reflectance of photonic crystals which have identical lattice constants but different diameters.

Fig. 7a shows NCPMs with particles of 710 nm in square, circle, and triangle shapes, surrounded by the CPM with particles of 780 nm, both on black adhesive tape. And measurements of reflectance show a decrease of approximately 10% from the CPM to the NCPM (Fig. 7b). This implies that matching the reflectance is necessary to achieve a covert feature in the hybrid label combining the CPM and NCPM. Therefore, we have conducted parametric studies on the reflectance of photonic crystals. Various monolayers of photonic crystals were prepared with the same lattice constant (780 nm) and different diameters (780, 710, 655,
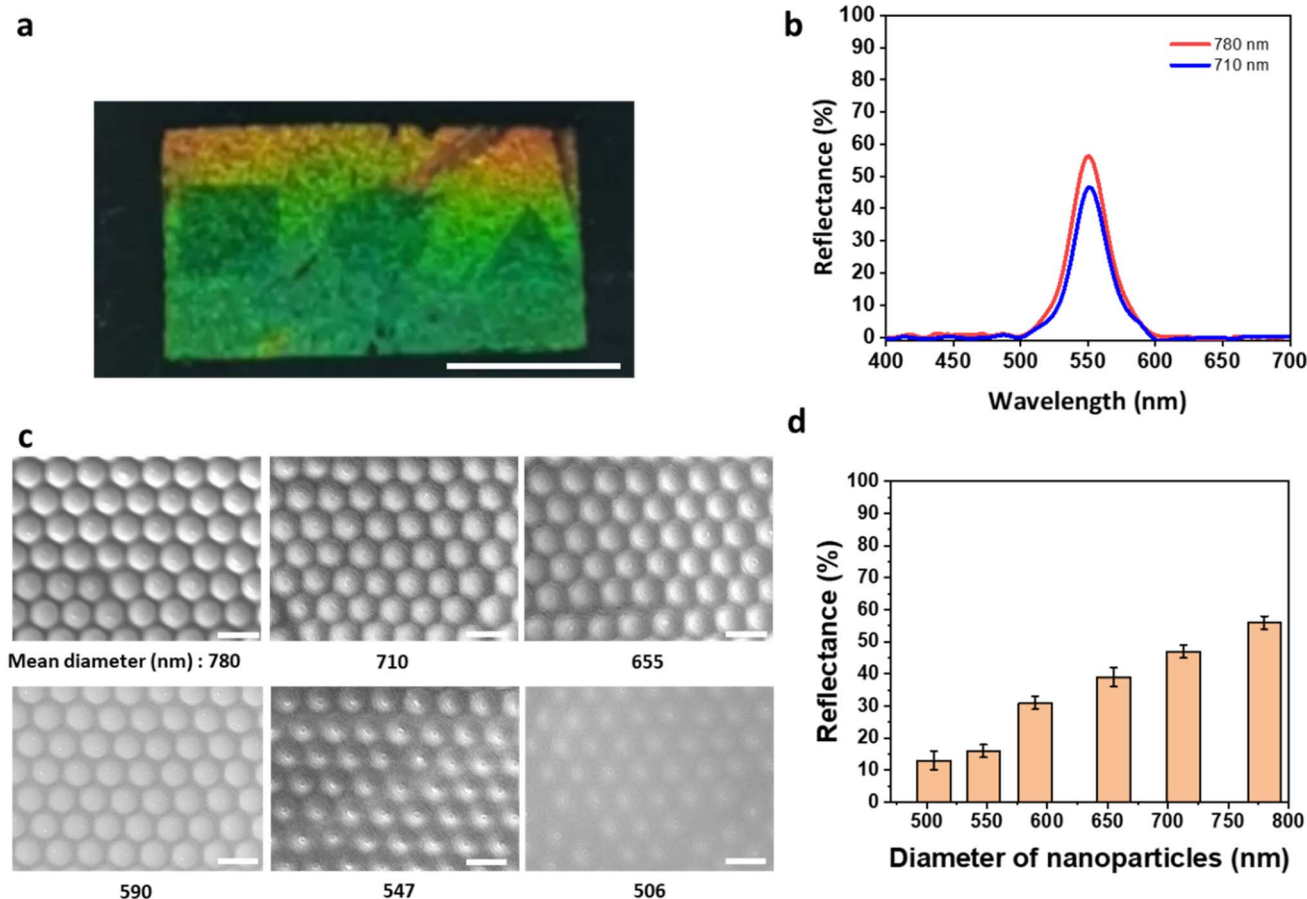

Fig. 7 (a) Photo (scale bar: 1 cm) and (b) reflectance spectrum of PCs with identical lattice constants but different particle diameters. (c) SEM images of various monolayers of PCs (scale bar: 1 μm) and (d) their reflectance. All PCs were fabricated on a black adhesive tape.

590, 547, 506 nm) on the adhesive black tape as seen in Fig. 7c and S3.† Then their reflectance was measured as seen in Fig. 7d. The reflectance decreased from 56% to 13% as the particle size decreased from its original diameter, 780 nm, to 506 nm.

This result suggests that the reflectance of the close-packed monolayer needs to be reduced while maintaining the diameter of particles. This can be achieved by adjusting the area fraction of the monolayer of the CPM during particle assembly. There has been a lot of literature investigating the assembly of particles and the formation of a monolayer by the spin coating technique.[40,41] When the particles are carried in liquid and their layer is made by the spin coating technique, the particles are attracted each other by capillary force, resulting in a close-packed layer. And if the spin speed is lower than the optimum value, excessive particles remain during the spinning process, resulting in multilayers of particles. Otherwise, if the spin speed is higher than optimum, monolayers are obtained but the lack of particles results in voids between monolayers. In Fig. 8a, dark areas at 600 and 800 rpm represent multilayers, and bright areas at 1200, 1400 and 1600 rpm represent the surface of wafer, or voids (Fig. S4†). From the perspective of reflectance, both multilayers and voids weaken the reflectance. However, the degradation caused by voids is greater than that caused by multilayers, as seen in Fig. 8b and c. It is because the multilayers still contribute to the generation of structural colors. As a result, the NCPM containing 710 nm particles matches the reflectance of the CPM with an 80% monolayer fraction. Therefore, the hybrid labels of the CPM and NCPM have been fabricated as seen in Fig. 9a and Video S7.† These labels have specific shapes containing the NCPM, which are hidden or encrypted until a cover film is applied. As the label is flexible, it is expected to be applied for anti-counterfeiting labels which need to be in deformation or curved surfaces. We applied the label onto a Vietnamese banknote to demonstrate practical applications. As shown in Fig. 9b, the label conformably adhered to the banknote even at a bent state (top image). Interestingly, the covert–overt feature was triggered using the PET cover film (top image) or the transparent area of the banknote (bottom image), demonstrating the convenience of this principle for anti-counterfeiting uses.
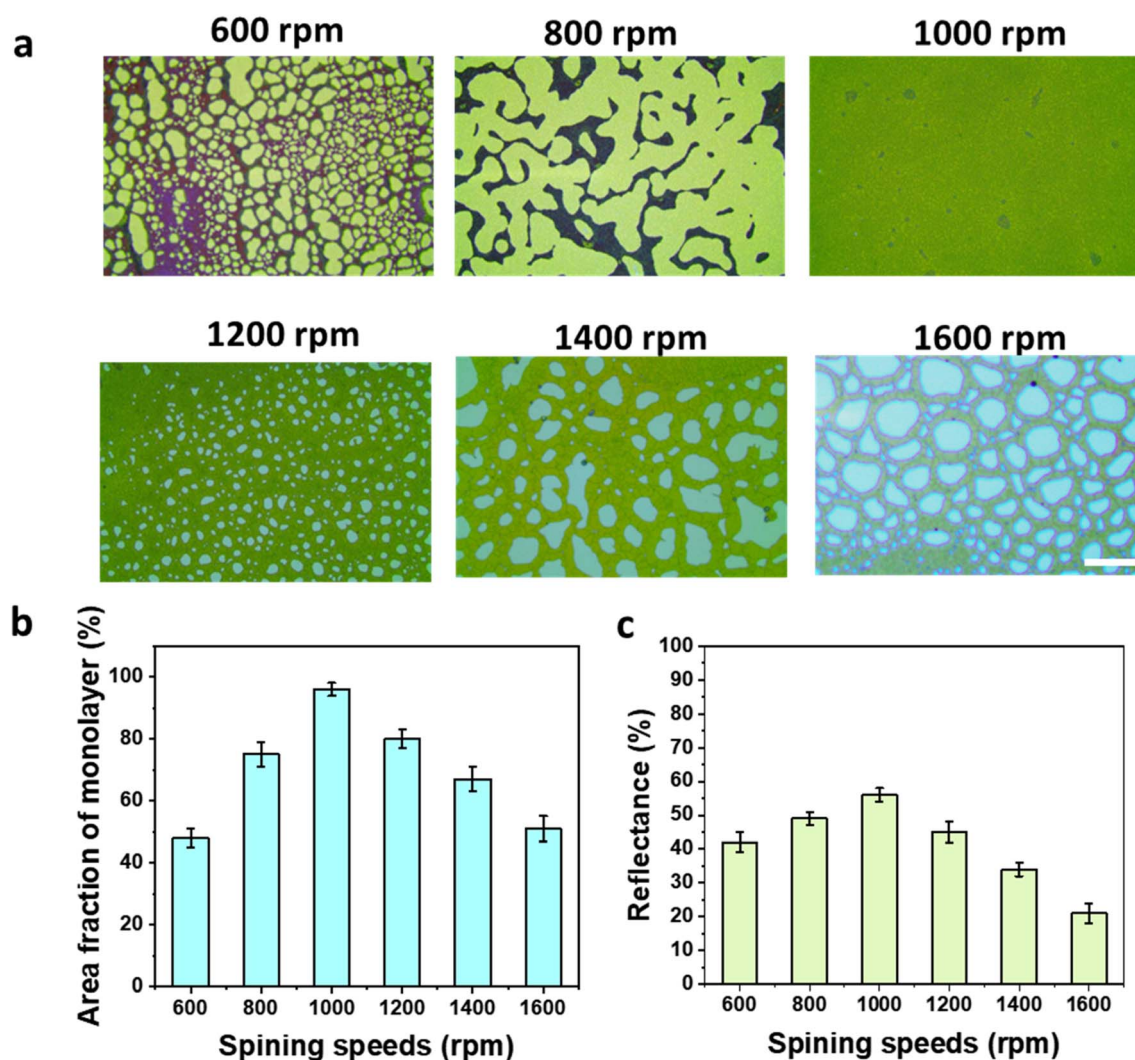

Fig. 8 (a) Optical microscopy images of particle layers on a silicon substrate for various spin speeds (scale bar: 100 μm), (b) area fraction of monolayers and (c) reflectance of particle layers for various spin speeds.
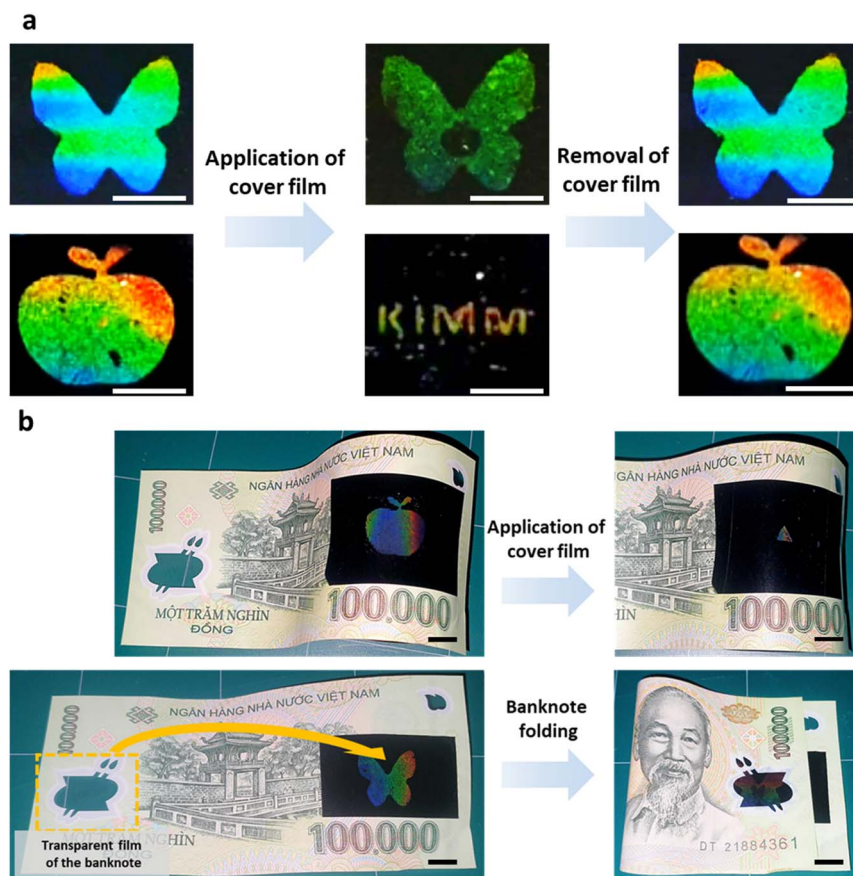
Fig. 9 (a) Hybrid labels containing the CPM and NCPM, (b) the hybrid labels on a Vietnamese banknote at a bent state (top image) and flat state (bottom image) (scale bar: 1 cm).

Conclusion

In this study, a simple and scalable fabrication process is introduced to obtain a close-packed monolayer and non-close-packed monolayer of nanoparticles for anti-counterfeiting applications. With the application of a transparent cover film, the NCPM was instantly hidden, while the CPM kept emitting colors. This occurred because the NCPM was embedded beneath the surface of a deformable adhesive tape, causing the cover film and tape to adhere together, while there was no interspace between particles in the CPM. The covert–overt PCs were also fabricated on dark and transparent tapes. It was shown that the covert label could be obtained on dark tape due to the high absorption of light, regardless of the refractive index. However, when a transparent tape was used, matching refractive indices of NPs and the tape was necessary. Based on this study, hidden labels that could only be revealed by peeling off the cover film or washing with water have been demonstrated for anti-counterfeiting usage. For higher security levels, the color and reflection of the CPM and NCPM were modulated to be nearly identical so that their integration provided a simple method to create encrypted labels. Furthermore, by tailoring properties of the adhesive layer or cover films, this principle can be utilized as indicators for

mechanical pressure or exposure to water or chemicals. The fabrication process in this study provides the flexibility for versatile photonic crystals, which is expected to have a broad impact on the commercialization of future anti-counterfeiting labels.

Data availability

The authors confirm that the data and findings of this study are available within the article and its ESI.† Raw data that support the findings of this study are available from the corresponding author, upon reasonable request.

Author contributions

N. H. M., J. S. Y. conceived and designed the experiments. N. H. M., K. K., D. H. K. carried out the experiments and analyzed the data. N. H. M. wrote the paper. Y. Y. commented on the manuscript. J. S. Y. revised and modified the manuscript.

Conflicts of interest

The authors declare no competing interests.

Acknowledgements

References

1 V. Maritano, P. Barge, A. Biglia, L. Comba, D. Ricauda Aimonino, C. Tortia and P. Gay, *J. Food Prot.*, 2024, **87**, 100251.

2 A. Ghadge, A. Duck, M. Er and N. Caldwell, *Supply Chain Forum Int. J.*, 2021, **22**, 87–99.

3 H. Huang, H. Li, J. Yin, K. Gu, J. Guo and C. Wang, *Adv. Mater.*, 2023, **35**, 2211117.

4 T. Wang, H. Zheng, C. You and J. Ju, *Sensors*, 2023, **23**, 795.

5 Y. Zhou, G. Zhao, J. Bian, X. Tian, X. Cheng, H. Wang and H. Chen, *ACS Appl. Mater. Interfaces*, 2020, **12**, 28532–28538.

6 R. Xie, C. Hong, S. Zhu and D. Tao, *Neurocomputing*, 2015, **167**, 625–635.

7 T. Zhang, L. Wang, J. Wang, Z. Wang, M. Gupta, X. Guo, Y. Zhu, Y. C. Yiu, T. K. C. Hui, Y. Zhou, C. Li, D. Lei, K. H. Li, X. Wang, Q. Wang, L. Shao and Z. Chu, *Nat. Commun.*, 2023, **14**, 2507.

8 A. K. Gangwar and D. K. Bharti, *Bull. Mater. Sci.*, 2023, **46**, 224.

9 S. Gandla, C. Moon, S. Baek, H. Park and S. Kim, *Adv. Funct. Mater.*, 2023, **33**, 2211762.

10 S. Teutoburg-Weiss, M. Soldera, F. Bouchard, J. Kreß, Y. Vaynzof and A. F. Lasagni, *Opt Laser. Technol.*, 2022, **151**, 108012.

11 M. Zhou, S. Chen, B. Wei, D. Yang, D. Ma and S. Huang, *J. Colloid Interface Sci.*, 2023, **650**, 313–321.

12 R. Zhang, Z. Yang, Q. Wang, W. Li, H. Xu and L. Li, *Dyes Pigm.*, 2023, **208**, 110794.

13 N. H. Minh, K. Kim, D. H. Kang, Y.-E. Yoo and J. S. Yoon, *Nanotechnology*, 2021, **32**, 495302.

14 C. Ji, M. Chen and L. Wu, *Adv. Opt. Mater.*, 2022, **10**, 2102383.

15 Q. Guo, X. Wang, J. Guo and C. Wang, *Nanoscale*, 2023, **15**, 18825–18831.

16 R. Li, S. Zhang and R. Zhang, *Chem.: Methods*, 2023, **3**, e202200081.

17 Y. Hu, Z. Tian, D. Ma, C. Qi, D. Yang and S. Huang, *Adv. Colloid Interface Sci.*, 2024, **324**, 103089.

18 H. S. Lee, T. S. Shim, H. Hwang, S.-M. Yang and S.-H. Kim, *Chem. Mater.*, 2013, **25**, 2684–2690.

19 Z. Meng, S. Wu, B. Tang, W. Ma and S. Zhang, *Nanoscale*, 2018, **10**, 14755–14762.

20 X. Zhang, Q. Fu and J. Ge, *Adv. Photonics Res.*, 2021, **2**, 2000208.

21 C. Xu, C. Huang, D. Yang, L. Luo and S. Huang, *ACS Omega*, 2022, **7**, 7320–7326.

22 W. Yu, Y. Zhao and J. Ge, *J. Colloid Interface Sci.*, 2024, **659**, 603–610.

23 H. Wang, H. Zhang, Z. Chen, Y. Zhao, Z. Gu and L. Shang, *Prog. Mater. Sci.*, 2023, **135**, 101091.

24 H. Han, J. W. Oh, H. Lee, S. Lee, S. Mun, S. Jeon, D. Kim, J. Jang, W. Jiang, T. Kim, B. Jeong, J. Kim, D. Y. Ryu and C. Park, *Adv. Mater.*, 2024, **36**, 2310130.

25 Y. Hu, D. Yang, D. Ma, C. Qi and S. Huang, *Adv. Funct. Mater.*, 2024, **34**, 2310861.

26 P. Ren, X. Chen, L. Sun, Q. Lyu, L. Zhang and J. Zhu, *ACS Appl. Mater. Interfaces*, 2022, **14**, 50190–50198.

27 C. Ji, M. Chen and L. Wu, *Adv. Opt. Mater.*, 2022, **10**, 2102383.

28 L. Chu, X. Zhang, W. Niu, S. Wu, W. Ma, B. Tang and S. Zhang, *J. Mater. Chem. C*, 2019, **7**, 7411–7417.

29 Y. Liu, G. Liu, Y. Wu, W. Cai, Y. Wang, S. Zhang, H. Zeng and X. Li, *Adv. Mater.*, 2023, **35**, 2301914.

30 Z. Zhang, H. Cheng, S. Teng, K. Huang, D. Wang, W. Yang and R. Xie, *Inorg. Chem.*, 2022, **61**, 20552–20560.

31 Q. Zhou, J. G. Park, J. Bae, D. Ha, J. Park, K. Song and T. Kim, *Adv. Mater.*, 2020, **32**, 2001467.

32 S. Ye, Q. Fu and J. Ge, *Adv. Funct. Mater.*, 2014, **24**, 6430–6438.

33 N. Hoang Minh, K. Kim, D. H. Kang, Y.-E. Yoo and J. S. Yoon, *ACS Appl. Nano Mater.*, 2024, **7**, 20361–20369.

34 Q. Kuang, X. Hou, C. Du, X. Wang and D. Gao, *Phys. Chem. Chem. Phys.*, 2023, **25**, 17759–17768.

35 Y. Gao, K. Ge, Z. Zhang, Z. Li, S. Hu, H. Ji, M. Li and H. Feng, *Advanced Science*, 2024, **11**, 2305876.

36 H. Huang, X. Wang, X. Li, Y. Li, G. Liu, L. Zhou and J. Shao, *Dyes Pigm.*, 2024, **221**, 111802.

37 D. Nagao, R. Kameyama, H. Matsumoto, Y. Kobayashi and M. Konno, *Colloids Surf., A*, 2008, **317**, 722–729.

38 Y. Wu, R. Sun, J. Ren, S. Zhang and S. Wu, *Adv. Funct. Mater.*, 2023, **33**, 2210047.

39 N. H. Minh, K. Kim, D. H. Kang, Y.-E. Yoo and J. S. Yoon, *Sci. Rep.*, 2022, **12**, 21926.

40 A. Chandramohan, N. V. Sibirev, V. G. Dubrovskii, M. C. Petty, A. J. Gallant and D. A. Zeze, *Sci. Rep.*, 2017, **7**, 40888.

41 S. Khanna, Utsav, P. Marathey, H. Chaliyawala, N. Rajaram, D. Roy, R. Banerjee and I. Mukhopadhyay, *Colloids Surf., A*, 2018, **553**, 520–527.